Electrochemical Self-Assembly of CuSCN/4-Cyano-4'-(*N*'-methyl)Stilbazolium Hybrid Thin Films

ECS Transactions, 97 (7) 457-469 (2020)
10.1149/09707.0457ecst ©The Electrochemical Society

Electrochemical Self-Assembly of CuSCN/4-Cyano-4'-(*N*'-methyl)Stilbazolium Hybrid Thin Films

Y. Tsuda[a], T. Suzuki[a], T. Nakamura[a], K. Uda[a], R. Yamakado[b], S. Okada[b], P. Stadler[b] and T. Yoshida[a] *

[a] Graduate School of Science and Engineering, Yamagata University, 4-3-16 Jonan, Yonezawa, Yamagata 992-8510, Japan
[b] Graduate School of Organic Materials Science, Yamagata University, 4-3-16 Jonan, Yonezawa, Yamagata 992-8510, Japan
[c] Institute of Physical Chemistry, Johannes Kepler University Linz, Altenbergerstrase 69 4040 Linz, Austria

Electrochemical self-assembly (ESA) of CuSCN/4-cyano-4'-(*N'*-methyl)stilbazolium (CNS^+) hybrid thin films has been performed and analyzed in comparison with CuSCN/4-(*N*,*N*-dimethylamino)-4'-(*N'*-methyl)stilbazolium (DAS^+) hybrid system. Due to the presence of strongly electron-withdrawing -CN group, CNS^+ has a much higher dipole moment than DAS^+ to exhibit stronger affinity to CuSCN. CNS^+ therefore gave strong impact to the crystal growth of CuSCN with its smaller concentration than DAS^+, such as changing crystal orientation, creating unique nanostructure and phase transition from β- to α-CuSCN. CNS^+ has been found to obey the same mechanism as DAS^+ for its loading into the film. The limit for diffusion limited loading was pushed up to its bulk concentration of 200 μmol dm^{-3}, much higher than that for DAS^+ (60 μmol dm^{-3}). Also, the efficiency of dye uptake in the surface reaction limited loading was enhanced about 3 times due to the improved stability of CuSCN/CNS surface complex.

Introduction

Inorganic/organic hybrid materials offer unlimited possibilities for novel functional materials. Intimate chemical and physical interaction between the inorganic and organic

constituents let us anticipate concerted new functionalities which is not expected solely by one of the two components. We have established “Electrochemical Self-Assembly (ESA)” as a way to obtain such functional inorganic/organic hybrid materials [1-2]. Organic molecules are loaded into inorganic host compound during its electrodeposition when there is a right chemistry between them.

ESA of ZnO/organic dye hybrid thin films is a good example [3]. Highly crystallized sponge-like nanostructured porous ZnO was obtained at a low temperature, which was ideally suited to processing photoanode materials for flexible dye-sensitized solar cells (DSSCs) [1]. Eosin Y bearing carboxylic acid group exhibits a high affinity to ZnO and thereby is loaded at a high amount not only to color the ZnO film but also significantly alter the morphology of ZnO. Anionic eosin Y should be replacing oxide and hydroxide ions of ZnO surface. Likewise, we have also discovered that many of cationic organic dyes afford ESA during cathodic electrodeposition of CuSCN [4], supposedly by replacing a part of Cu(I) cations. CuSCN is a wide bandgap p-type semiconductor finding use as a hole transporting material in solar cells, whereas ZnO is a typical widegap n-type. Thus, ESA of these ZnO/anionic dye and CuSCN/cationic dye hybrid thin films present very good complementarity.

Concerted photoluminescence (PL) has been observed for CuSCN/4-(*N*,*N*-dimethylamino)-4’-(*N*’-methyl)stilbazolium (DAS, Fig. 1 (a)) hybrid thin film prepared by ESA, in which PL from DAS is enhanced by energy transfer from CuSCN matrix [5]. Highly polar rod-like DAS cations are supposedly aligned and well-packed on the SCN^- terminated *c*-planes of rhombohedral *β*-CuSCN [6], resulting in an exciton stabilization to exhibit PL, rather than its quenching by charge transfer as observed in dye-sensitized systems. Such ordered attachment of DAS also has resulted in evolution of unique nanostructures of CuSCN [6]. Tiny hybrid nanostructure with a high DAS loading turned out to exhibit efficient energy transfer with a high CuSCN/DAS interface. Thus, understanding the mechanism of dye loading is crucially important to find out the conditions to obtain materials with high functionalities.

Electrochemical analysis employing a rotating disk electrode (RDE) combined with compositional analysis of the product thin films revealed switching of DAS loading from diffusion limited process to that limited by the surface reaction for the formation of CuSCN/DAS complex, depending on the concentration of DAS (C_{DAS}), whereas the electrodeposition of CuSCN always occurs as limited by transport of its precursor, i.e., $[Cu(SCN)]^+$ complex [7]. DAS is occluded into the CuSCN grains when its loading is limited by diffusion, whereas they are phase separated to show efficient PL, when the surface reaction operates for hybridization [5]. The border for the switching of dye

loading mechanism was found as the ratio between bulk concentrations of dye and the $[Cu(SCN)]^+$ complex, C_{DAS}/C_{comp} = ca. 1/31 in case of DAS [8].

While it is important to verify the above-mentioned mechanism, a cationic stilbazolium dye similar to DAS but with a higher affinity with SCN^- should result in the switching C_{dye}/C_{comp} ratio higher than that for DAS. In this study, we have employed 4-cyano-4'-(*N*'-methyl)stilbazolium (CNS, Fig. 1 (b)) to test the idea. Strongly electron withdrawing cyano group is introduced in CNS, so that it should result in a clearly larger dipole moment than that of DAS, and thereby should more strongly interact with SCN^- ions. In this paper, preliminary results of the electrochemical and compositional analysis are reported for the ESA of CuSCN/CNS hybrid thin films.

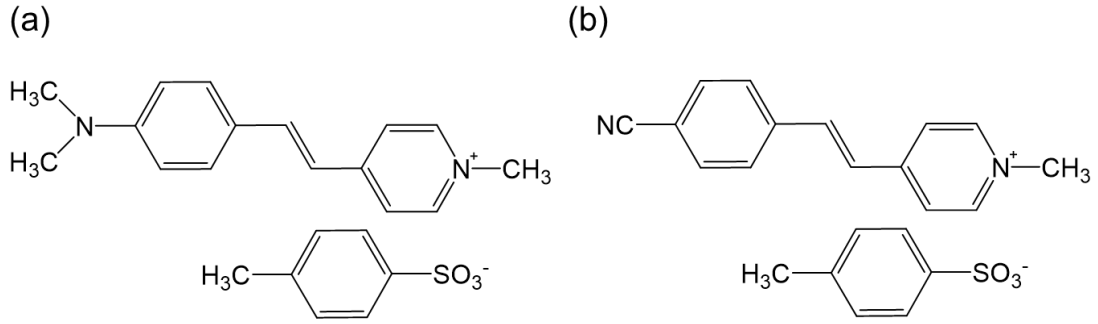

Figure 1. Structure of 4-(*N*,*N*-dimethylamino)-4'-(*N*'-methyl)stilbazolium tosylate (DAST) (a) and 4-cyano-4'-(*N*'-methyl)stilbazolium tosylate (CNST) (b).

Experimental

Copper(II) perchlorate hexahydrate ($Cu(ClO_4)_2 \cdot 6H_2O$, 98%, Aldrich), lithium thiocyanate dihydrate ($LiSCN \cdot 2H_2O$, 95%, Kishida), lithium perchlorate ($LiClO_4$, 98%, Wako) and methanol (99.8%, Wako) were used as purchased. Crystalline powder of 4-cyano-4'-(*N*'-methyl)stilbazolium tosylate (CNST) was synthesized according to the procedure published elsewhere [9]. Density functional theory (DFT) calculation was carried out to estimate the dipole moments of CNS^+ as well as DAS^+ in methanol (PCM-B3LYP/6-311+G(d,p)//B3LYP/6-31G(d,p)).

The electrolytic bath was prepared to contain 0.1 mol dm^{-3} LiSCN as supporting electrolyte, 2.5 mmol dm^{-3} $Cu(ClO_4)_2 \cdot 6H_2O$, 2.5 mmol dm^{-3} $LiSCN \cdot 2H_2O$ and CNST at various concentrations (C_{CNS}) between 0 and 1000 μmol dm^{-3} in methanol. F-doped tin oxide (FTO) coated conductive glass substrate (Asahi-DU 10 Ω/sq.) cut into 20 × 35 mm was cleaned sequentially in Decon® detergent, acetone, and 2-propanol

ultrasonically for storage. It was activated in a 45% HNO_3 for 2 min and rinsed with distilled water just before it was attached to a home-made rotating disk electrode (RDE) via a specially designed attachment. A circular aperture with a 14 mm diameter (electrode area = 1.54 cm^2) centered to the rotating axis was achieved by a masking tape (Nitto Denko N-380). A Pt wire and an Ag/AgCl electrode served as counter and reference electrodes, respectively [8]. CuSCN and CuSCN/CNS hybrid thin films were electrodeposited under a transport-limited regime [10] by cathodizing the FTO working RDE (ω = 500 rpm) at +0.2 V vs. Ag/AgCl for 180 s at room temperature (298 K). An electrochemical measurement system (Hokuto Denko HSV-110) was employed for the electrolysis and recording chronoamperograms. The product thin films were rinsed with pure water, dried in air at room temperature, and subjected to further analyses. Transmission UV–Vis absorption spectra were measured on a SHIMADZU SolidSpec-3700 spectrophotometer. Surface morphology was observed by HITACHI SU8000 field emission scanning electron microscope (FE-SEM). X-ray diffraction (XRD) patterns in θ- 2θ scans were measured on a RIGAKU RINT Ultima-IV X-ray diffractometer.

In order to check the location of CNS, namely, CNS either entrapped in CuSCN or phase separated from CuSCN, the electrodeposited hybrid thin films were soaked in *N*,*N*-dimethylacetamide (DMA) at room temperature for overnight. The level of CNS extraction has been determined by measuring transmission absorption spectra before and after the DMA treatment.

The absolute amount of CNS loaded into the films was determined by dissolving the entire product film (1.54 cm^2 projected area) into a 10 ml of 7 mol dm^{-3} ammonia and measuring its absorption spectrum for the peak of CNS (λ = 334 nm, $\varepsilon = 3.6 \times 10^4$ M^{-1} cm^{-1} in ammonia). The amount of electrodeposited CuSCN has also been estimated spectroscopically according to Lambert-Beer's Law by measuring the absorbance for the *d-d* transition of $[Cu(NH_3)_4]^{2+}$ complex (λ = 638 nm, ε = 137 M^{-1} cm^{-1} as determined separately by dissolving $Cu(ClO_4)_2$ in 7 mol dm^{-3} ammonia).

Result and discussion

Introduction of a strongly electron withdrawing -CN group resulted in a greatly increased dipole moment of 23.5016 Debye for CNS^+ in methanol, compared to 10.1442 Debye for DAS^+ as determined by DFT calculation. In fact, HOMO-LUMO gap of CNS^+ is also greatly enlarged to make it bright yellow (λ_{max} = 334 nm), whereas DAS^+ is intensely red (λ_{max} = 455 nm), since these rod-like stilbazolium dyes undergo

intramolecular charge transfer upon photoexcitation. The increased dipole moment, in return, let us anticipate increased interaction of CNS^+ with CuSCN (essentially with SCN^- ion), although direct precipitation has not been observed upon addition of CNST to the electrolytic bath for CuSCN. Successful preparation of homogeneous mixture just like the case with DAST allowed us to test ESA of CuSCN/CNS hybrids.

While colorless crystalline *β*-CuSCN thin film is obtained without addition of dyes, yellow colored thin films are obtained in the presence of CNST. This itself is already an indication of successful loading of CNS^+ during the electrodeposition of CuSCN. Increasing CNST concentration in the bath roughly increased the yellowness of the films, making the overall behavior quite similar to those observed in the ESA of CuSCN/DAS. Fig. 2a shows chronoamperograms during the electrodeposition upon increasing concentration of CNST (C_{CNS}). The current stays constant for about -0.9 mA cm^{-2} without CNST, as the electrodeposition of CuSCN is solely limited by the transport of the precursor complex,

$$[Cu(SCN)]^+ + e^- \rightarrow CuSCN \quad (1)$$

Almost the same holds up to 100 μM CNST, except slight decrease of the steady-state current. Upon higher addition, however, initial rise of current begins to appear. For CNST higher than 500 μM, a sort of incubation time appears in the beginning of the electrolysis. The current almost stays minimal of about 0.02 mA cm^{-2} for a period and then takes off to achieve certain steady-state current. On further increasing the CNST concentration, this incubation period is extended, associated with a clear decrease of the steady-state current. In fact, similar influence has been observed for DAS^+ but in much lesser extent (Fig. 2b). The incubation period appears only on extreme addition of DAST and the decrease of the initial as well as the steady-state current is not as strong as that with CNST. We have confirmed that the amount of electrodeposited CuSCN is always proportional to the consumed charge irrespective of dye addition, so that the observed cathodic current is dominated by that of Eq. (1). A possible explanation for the decrease of the steady-state current is the decrease of the effective concentration of $[Cu(SCN)]^+$ by forming complex with the added dyes. However, the decrement is not proportional to the added dye concentration both for CNST and DAST. It also doesn't explain the initial rise of current following the incubation time. It is likely that the charge transfer reaction for Eq. (1) is kinetically hindered in the presence of these dyes in very high concentration. The kinetic hindrance is then obviously much stronger for CNST than DAST. Small current during the incubation period might be resulting in accumulation of some chemical species at the electrode surface. Then, reaction sites (most likely CuSCN crystallites) are formed for charge transfer to $[Cu(SCN)]^+$ which is readily available at the vicinity of the electrode

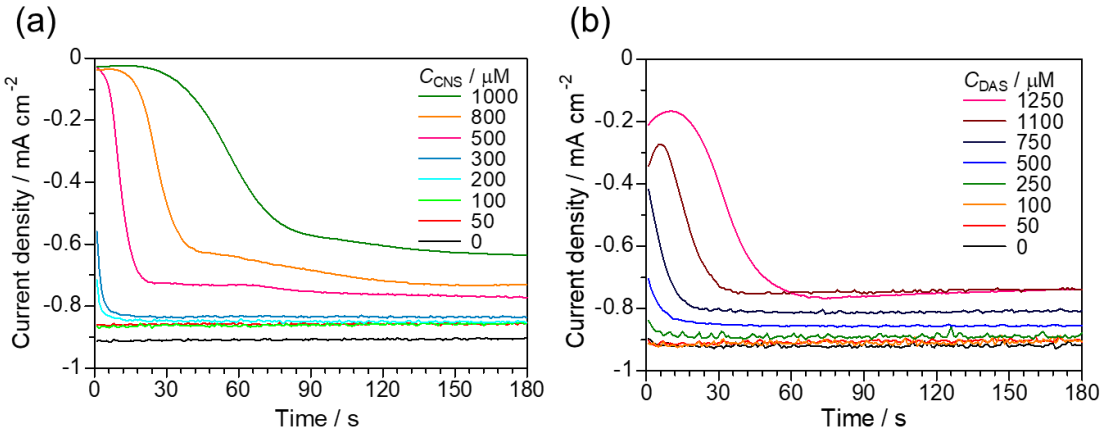

Figure 2. Chronoamperograms during cathodic electrodeposition of CuSCN/CNS (a) and CuSCN/DAS (b) hybrid thin films at +0.2 V (vs. Ag/AgCl), 500 rpm and for 180 s in methanolic solutions containing 2.5 mmol dm^{-3} $Cu(ClO_4)_2$ 2.5 mmol dm^{-3} LiSCN and 0.1 mol dm^{-3} $LiClO_4$ with variation of C_{CNS} = 0-1000, C_{DAS} = 0-1250 μmol dm^{-3}, respectively.

surface. Consequently, the current rises as the reaction sites increases and reaches plateau when the electrode is fully covered with the hybrid films.

XRD patterns of the electrodeposited CuSCN and CuSCN/CNS hybrid thin films are shown in Fig. 3. While dye-free thin film is that of *β*-CuSCN, preferentially oriented with its *c*-axis perpendicular to the substrate as indicated from its enhanced (003) peak compared to the JCPDS data, minor addition of CNST lays down the *c*-axis in parallel with the substrate as recognized by the increased (101) peak intensity on sacrifice of (003), since (101) is close to parallel with the *c*-axis at 11.48° for the hexagonal superlattice structure of *β*-CuSCN elongated for the *c*-axis (lattice constants; $a,b = 3.857$ Å, $c = 16.449$ Å) [11]. Then, further addition of CNST up to 300 μM results in decrease and broadening of the diffraction peaks. Above 500 μM, diffraction peaks assignable to orthorhombic *α*-CuSCN are recognized. These changes of crystal orientation, broadening and phase transition from *β* to *α* form are essentially the same observations as those reported for the ESA of CuSCN/DAS, although the changes occurred at higher concentrations of DAST than CNST. The stronger impact of CNS^+ to the crystal growth of CuSCN than DAS^+ should also be an indication of its stronger affinity to CuSCN surface.

The modification of the crystal growth by attachment of CNS^+ leads to associated changes of the film morphologies (Fig. 4). Pure CuSCN thin film is made of rugged particles to form a rough and open morphology, which is indicative of surface reorganization by dissolution/recrystallization sequence, since diffusion controlled highly irreversible precipitation should result in a flat surface. Small addition of CNST at 50 μM dm^{-3} indeed made the film denser and flatter, since stable attachment of CNS^+, in return,

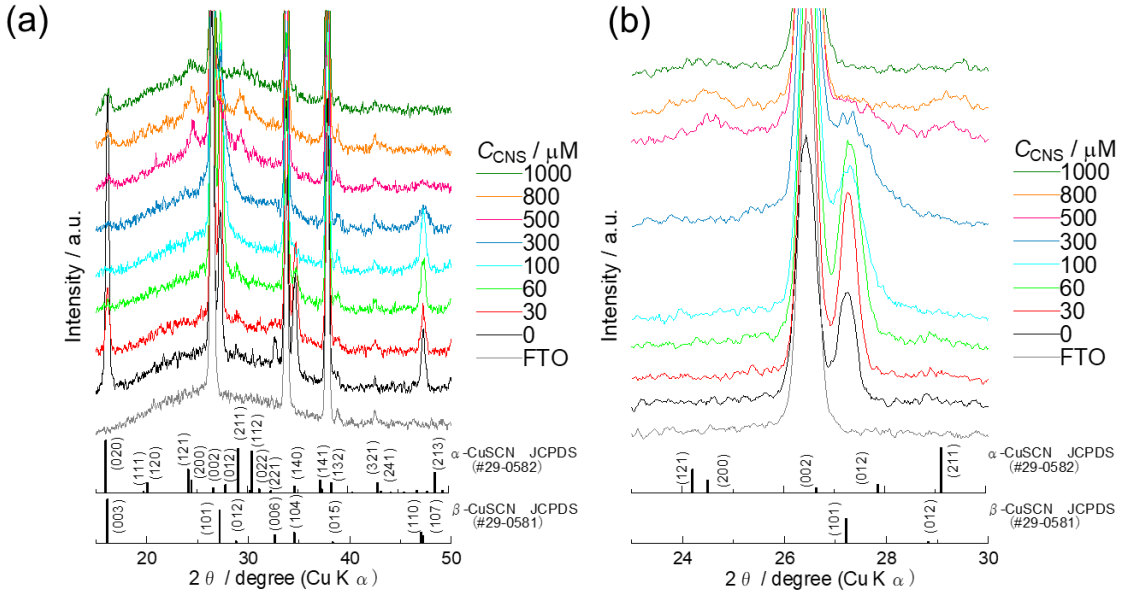

Figure 3. XRD patterns of electrodeposited CuSCN/CNS hybrid thin films with C_{CNS} = 0-1000 μmol dm^{-3} shown for wide angle (a) and close-up for 2θ = 23-30° (b), in comparison with that of the bare FTO substrate and powder diffraction standards of α- and β-CuSCN.

should stabilize CuSCN against dissolution. This change of morphology should also be associated with the high degree of anisotropy to orient the *c*-axis of β-CuSCN in parallel with the substrate as found by the XRD for this film. At C_{CNS} = 300 μmol dm^{-3}, distinctive nanostructure of elongated and flat-laid nanorod is recognized. This morphology is somewhat similar to the unique "hair comb" nanostructure previously observed for the CuSCN/DAS hybrid thin films grown with similar dye concentration range. As it is shown later, the loaded CNS^+ becomes extractable by solvent because of phase separation from CuSCN, while CNS^+ is entrapped in CuSCN grain for those grown with lower C_{CNS}. With the highest end of C_{CNS} = 1000 μmol dm^{-3}, the morphology changes dramatically again. As discussed from the XRD data, phase transition to orthorhombic α-CuSCN occurs for this C_{CNS} range. Dense and large grains with round top are seen, for which internal scale-like nanostructure is found due to phase separation of the loaded CNS^+ from CuSCN. These observations about the change of the morphology on increasing CNST concentration, also linked to the crystallographic change, are in good accordance with those found for the CuSCN/DAS hybrid thin films [6]. Therefore, it is safe to consider the same behavior of CNS^+ as DAS^+ in its ESA with CuSCN.

The UV-vis transmission absorption spectra of the thin film samples are shown in Fig. 5. Since high addition of CNST resulted in clear decrease of consumed charge, and thereby the amount of electrodeposited CuSCN for a given period of the electrolysis, the

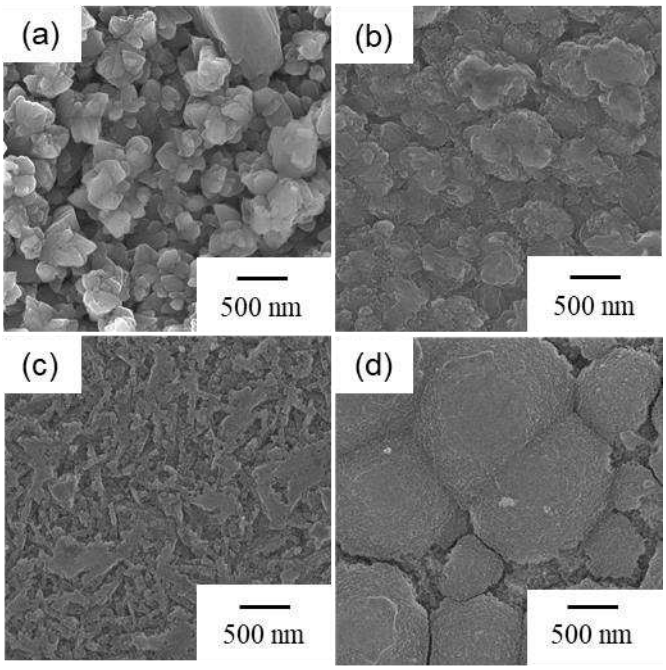

Figure 4. SEM pictures of CuSCN and CuSCN/CNS hybrid thin films electrodeposited with 0 (a), 50 (b), 300 (c) and 1000 µmol dm^{-3} (d) CNST.

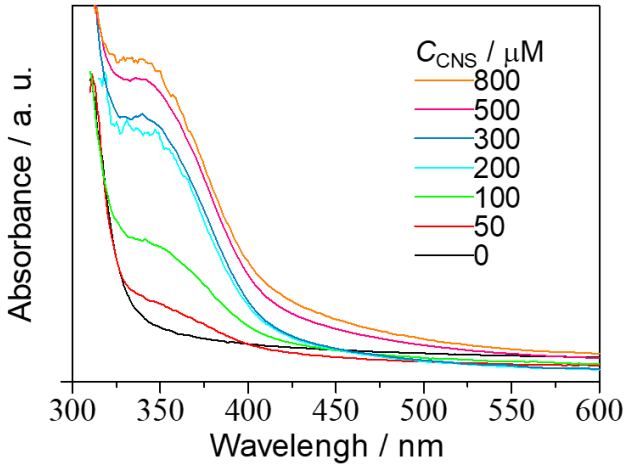

Figure 5. UV-vis absorption spectra of CuSCN and CuSCN/CNS hybrid thin films electrodeposited with 0, 50 100, 200, 300, 500 and 800 µmol dm^{-3} CNST. The absorbance was normalized by dividing with consumed charge to clarify the difference of CNS concentration in the hybrid thin films.

measured absorbance was divided by the consumed charge in order to clarify the difference of the concentration of CNS^+ loaded into the films. Pure CuSCN thin film is colorless, showing an absorption onset around 340 nm for its bandgap absorption, whereas the hybrid thin films exhibit absorption peaks around 350 nm due to the presence of CNS^+. Dye absorption increases monotonously, but not proportionally, on increasing

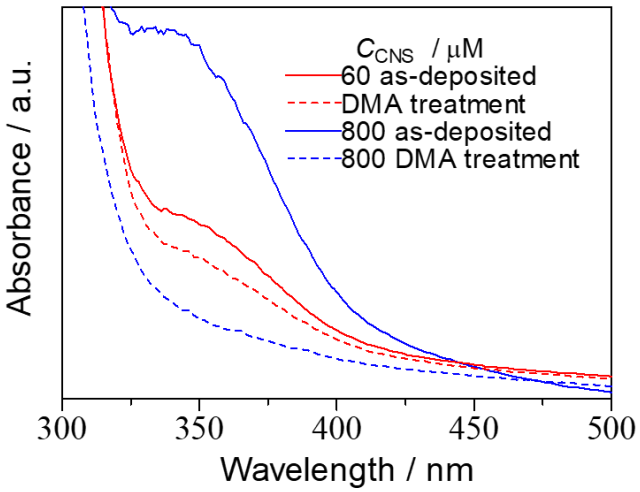

Figure 6. UV-vis absorption spectra of CuSCN/CNS hybrid thin films before and after the DMA treatment for C_{CNS} = 60 (dye entrapped) and 800 (dye segregated) μmol dm^{-3}. The absorbance was normalized by dividing with consumed charge to clarify the difference of CNS concentration in the hybrid thin films.

the CNST concentration in the bath. Clearly broadened and red-shifted absorption profile of CNS^+ in the hybrid thin film as compared to that in solution (λ_{max} = 334 nm) should be caused by the strong interaction with the CuSCN matrix.

The location of dyes, whether occluded in the CuSCN grains or phase separated as dye solid, can be studied by soaking the hybrid thin films in dimethylacetamide (DMA), since DMA doesn't dissolve CuSCN but is a good solvent for CNST [6]. The absorption spectra before and after the DMA treatment are shown in Fig. 6. While the hybrid thin film grown at C_{CNS} = 60 μmol dm^{-3} shows only about 30% decrease of the shoulder absorbance due to partial removal of CNS^+, the one with a high dye loading grown at C_{CNS} = 800 μmol dm^{-3} is totally bleached, since CNS^+ ions are segregated from CuSCN and thus are accessible by DMA for extraction. Such change of the hybrid structures from dye entrapment to separation was caused by the switching from diffusion limited dye loading to surface reaction limited dye loading for the ESA of CuSCN/DAS [8]. The same appears to be true in case of CuSCN/CNS in this study. However, the switching of the dye loading mechanism is expected to occur at a higher dye concentration due to the stronger interaction of CNS^+ than DAS^+.

The above-mentioned expectation was nicely confirmed to be true by plotting the total amount of precipitated dyes divided by the consumed charge (P_{CNS}, P_{DAS}) against dye concentration in the bath (C_{CNS}, C_{DAS}) (Fig. 7). For low dye concentration range, both P_{CNS} and P_{DAS} increases steeply proportional to C_{CNS} and C_{DAS}, as the dye loading is limited by diffusion [8]. In this regime, the electrodeposition of CuSCN is also diffusion

limited with minimal change of current during the electrolysis. Therefore, the amounts of precipitated CNS^+ and DAS^+ are also proportional to time. From the proportionalities of dye precipitation rate to the bulk concentration of dyes as 2.35 and 1.84 s^{-1}, diffusion coefficients of 1.60×10^{-6} and 1.25×10^{-6} cm^2 s^{-1} have been determined for CNS^+ and DAS^+, respectively, following the Levich relationship for diffusion limited dye precipitation described as,

$$P_{\mathrm{dye}} = 0.62 \times {D_{\mathrm{dye}}}^{\frac{2}{3}} \times \nu^{-\frac{1}{6}} \times \omega^{\frac{1}{2}} \times C_{\mathrm{dye}} \qquad (2)$$

where, D_{dye} is the diffusion coefficient of dye, ν is the kinetic viscosity of the solvent (0.687×10^{-4} cm^2 s^{-1} for methanol at 298 K [12]), ω is angular speed of rotation (52.4 rad s^{-1}) of RDE and C_{dye} is the bulk concentration (mol cm^{-3}) of dye. Then, P_{CNS} and P_{DAS} level off at approximately C_{CNS} = 200 μmol dm^{-3} and C_{DAS} = 60 μmol dm^{-3}, respectively, to fall down to other linearities with much smaller slopes. One should pay attention that the amount of dye precipitated per time (= dye precipitation rate) is no longer constant over the deposition period because of the incubation time due to kinetic hindrance, especially being strong for CNS^+. However, the amount of dye per charge, thus per precipitated CuSCN appeared constant in this high dye concentration regime. This is reasonably expected for the surface reaction limited loading of dyes [8]. Newly formed CuSCN provides sites for coordination of dyes. The stability of such surface complex should determine the efficiency of dye uptake. In this regard, clear enhancement is confirmed for the concentration of CNS^+ in the hybrid thin film being about 3 times larger than that of DAS^+ for a given dye concentration in the bath. Also, the slope of the plot for the surface reaction limited regime appears about 41.5% steeper for CNS^+ than DAS^+. These enhancements clearly indicate stronger coordination of CNS^+ than DAS^+. Because of its strong affinity, the border between diffusion limited and surface reaction limited ranges was pushed up to C_{CNS} = 200 μmol dm^{-3}, clearly higher than that for DAS^+.

Although we need to carry out a lot of elaborative experimental work to complete the analysis to identify the switching border as $C_{\mathrm{dye}}/C_{\mathrm{comp}}$ ratio for the loading of CNS^+ [8], the present preliminary analysis already nicely confirms that CNS^+ obeys the same mechanism as DAS^+ for its ESA with CuSCN. As expected from its high dipole moment, CNS^+ enlarges its diffusion limited loading up to a high dye concentration and also results in more stable surface complex in its surface reaction limited loading than DAS^+.

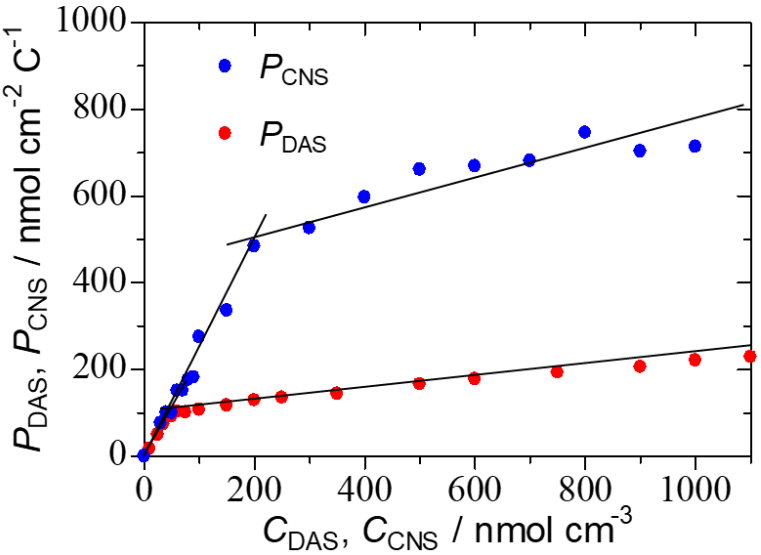

Figure 7. Total amount of dyes loaded into the hybrid thin films per consumed charge (P_{CNS}, P_{DAS}) by 180 s electrodeposition, plotted against the bulk concentrations of dyes (C_{CNS}, C_{DAS}) in the electrolytic bath.

Conclusion

ESA of CuSCN/CNS hybrid thin films was performed and analyzed for comparison with CuSCN/DAS system we studied before. The overall behavior of CNS^+ has been found exactly the same as DAS^+, so is the mechanism of dye loading during the film growth. Because of much higher dipole moment of CNS^+ than DAS^+, however, small concentration of CNS^+ already gave the influence to the crystal growth of CuSCN, such as changing the crystal orientation of β-CuSCN to lay down its c-axis and phase transition from β- to α-CuSCN. The regime for diffusion limited loading of CNS^+ was enlarged, pushing the border to switch to surface reaction limited loading to C_{CNS} = 200 μmol dm^{-3}, much higher than that for DAS^+ (C_{DAS} = 60 μmol dm^{-3}). The increased stability of CuSCN/CNS surface complex also resulted in about 3 times more efficient dye uptake in the surface reaction limited regime.

A lot more experimental elaboration, that includes film synthesis on variation of C_{comp} and ω, is needed to complete the analysis to express the switching border as C_{dye}/C_{comp} ratio. It is also desirable to express the surface reaction in a quantitative fashion. However, the present preliminary study already nicely confirmed the validity of our model. Having also found another stilbazolium dye, probably having a smaller dipole moment than DAS^+, we should be able to reach comprehensive understanding of ESA

of CuSCN/dye hybrids.

Acknowledgement

The present work was financially supported by Grant-in-Aid for Scientific Research (Kakenhi B, 18H02068) from Japan Society for the Promotion of Science (JSPS), Japan-Ukraine Bilateral Joint Research Project (Organic/inorganic hybrid crystals for NIR to visible upconversion) jointly funded by JSPS and the State Fund for Fundamental Research of Ukraine (project F80/39904) and Grant-in-Aid for JSPS Fellows Grant Number JP19J20693.

References

1. T. Yoshida, J. Zhang, D. Komatsu, S. Sawatani, H. Minoura, T. Pauporté, D. Lincot, T. Oekermann, D. Schlettwein, H. Tada, D. Woehrle, K. Funabiki, M. Matsui, H. Miura, H. Yanagi, *Adv. Func. Mater.*, **19**,17-43 (2009).
2. T. Oekermann, T. Yoshida, H. Minoura, K. G. U. Wijayantha and L. M. Peter, *J. Phys. Chem. B*, **108**, 8364-8370 (2004).
3. T. Yoshida and H. Minoura, *Adv. Mater.*, **12**, 1219-1222 (2000).
4. Y. Tsuda, K. Uda, M. Chiba, H. Sun, L. Sun, M. S. White, A. Masuhara, T. Yoshida, *Microsys. Technol.*, **24**, 715-723 (2018).
5. K. Uda, Y. Tsuda, S. Okada, R. Yamakado, L. Sun, Y. Suzuri, M. S. White, M. Furis, P. Stadler, O. P. Dimitriev, T, Yoshida, *ACS Omega*, **4**, 2, 4056-4062 (2019).
6. Y. Tsuda, H. Sun, L. Sun, S. Okada, A. Masuhara, P. Stadler, N. S. Sariciftci, M. S. White, T. Yoshida, *Monatsh. Chem.*, **148**, 845-854 (2017).
7. L. Sun, K. Ichinose, T. Sekiya, T. Sugiura, T. Yoshida, *Physics Procedia*, **14**, 12-24 (2011).
8. Y. Tsuda, T. Nakamura, K. Uda, S. Okada, R. Yamakado, L. Sun, Y. Suzuri, P. Stadler, O. Dimitriev, T. Yoshida, *J. Electrochem. Soc.*, **166** (9), B3098-B3102 (2019)
9. A. P. Phillips, *J. Org. Chem.*, **14**, 302-305 (1949).
10. K. Okabe, Y. Selk, T. Oekerman, T. Yoshida, *Trans. Mater. Res. Soc. Jpn*., **33**, 1325-1328 (2008).
11. Joint Committee on Powder Diffraction Standard, JCPDS No. 29-0581.

12. J. A. Dean, *Lange's Handbook of Chemistry*, Chapter 5, 15th Edn., McGraw-Hill Inc., New York (1999).